ELSEVIER

Materials Science and Engineering B 127 (2006) 239–250

MATERIALS SCIENCE & ENGINEERING B

www.elsevier.com/locate/mseb

InN growth by high-pressures chemical vapor deposition: Real-time optical growth characterization

Vincent Woods, Nikolaus Dietz *

Department of Physics & Astronomy, Georgia State University, Atlanta, GA, USA

Received 21 December 2004; received in revised form 23 October 2005; accepted 25 October 2005

Abstract

Growth techniques that utilize elevated reactor pressures offer a pathway to overcome limitations in the epitaxy of high quality group III-nitride compounds such as InN or related materials, which exhibit large thermal decomposition pressures. We introduce the growth of InN by a unique high-pressure chemical vapor deposition (HPCVD) system, demonstrating that HPCVD is a valuable method for achieving stoichiometric single-phase surface compositions at optimal processing temperatures. The development and utilization of real-time optical diagnostics for the monitoring of gas-phase and surface chemistry during the heteroepitaxial nucleation and growth is critical for controlling the chemical vapor deposition process. Using real-time optical ultraviolet absorption spectroscopy (UVAS), we have studied the flow and decomposition kinetics of the gas-phase precursors as functions of flow, pressure and temperature. A pulsed-injection technique for the delivery of the chemical precursors is used, enabling the analysis and control of the decomposition kinetics of trimethylindium (TMI) and ammonia as well as the study of the initial stages of InN nucleation and subsequent overgrowth on sapphire substrates. The nucleation and steady state growth of InN is probed with sub-monolayer resolution by principal angle reflectance (PAR) spectroscopy. These real-time optical monitoring techniques demonstrate their utility in the optimization and engineering of the growth process, as well as providing crucial insights into gas phase decomposition dynamics and surface chemistry processes under HPCVD conditions. The resulting InN material exhibits an optical absorption edge that varies from 0.83 to 1.34 eV, strongly dependent upon the precursor flow ratios employed during growth. Structural analysis performed by XRD reveals high quality InN.

Keywords: High-pressure CVD; Gas-phase kinetics; Real-time growth monitoring; InN growth

1. Introduction

The development of integrated ultraviolet (UV) light emitting diodes (LEDs), laser diodes, solar blind detectors, high-frequency/high-power transistors operating at high temperature and room-temperature spintronic devices that are based on group III-nitride compound semiconductors has generated much interest in recent years. Of particular interest is an improved knowledge of the binary base systems InN, GaN and AlN, and to which extent alloys and heterostructures can be employed in the fabrication of optical electronic device structures [1,2]. GaN is the most studied group III-nitride compound, but InN and AlN have become increasingly significant due to their unique properties as low band gap and wide band gap materials, respectively.

At present, the most commonly utilized growth techniques for the production of group III-nitrides are organometallic chemical vapor deposition (OMCVD, also denoted as MOVPE) and molecular beam epitaxy (MBE) [3,4]. However, these low-pressure deposition processes are limited to a temperature range under which the partial pressures of the constituents do not differ vastly and decomposition processes can be countered by off-equilibrium conditions. These off-equilibrium conditions employed in MBE and organometallic CVD growth of InN require a relatively low growth temperatures in order to overcome the thermal decomposition pressures, thus limiting the quality of InN and related group III-nitride epilayers [1,5–7]. In addition, these low growth temperatures require the application of extremely high V–III ratios in order to prevent the formation of metal droplets on the thin film surface. Recent studies pertaining to the decomposition of InN layers [8] have shown that oxygen is easily incorporated into the InN crystal under thermal treatments, and has been suggested as the source for the wide discrepancy in reports in the band gap energy of InN. Controversial reviews of the present status of InN growth and characterization have been provided by Bhuiyan et al. [1] and Davydov et al. [9], implying that different approaches for the

* Corresponding author. Tel.: +1 404 463 9617; fax: +1 404 651 1427.
E-mail address: ndietz@gsu.edu (N. Dietz).

0921-5107/$ – see front matter © 2005 Elsevier B.V. All rights reserved.
doi:10.1016/j.mseb.2005.10.032

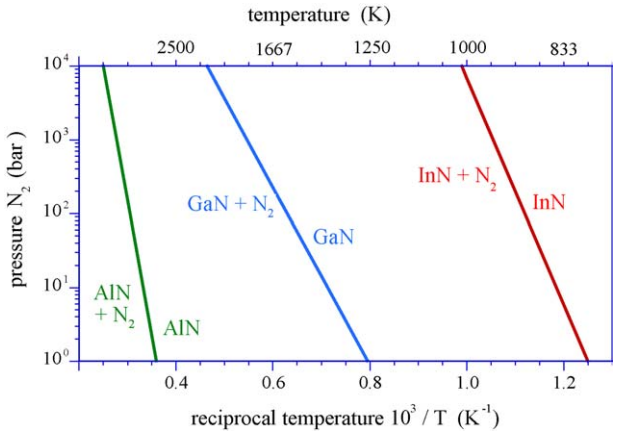

Fig. 1. Thermal decomposition pressure vs. reciprocal temperature for AlN, GaN and InN [11].

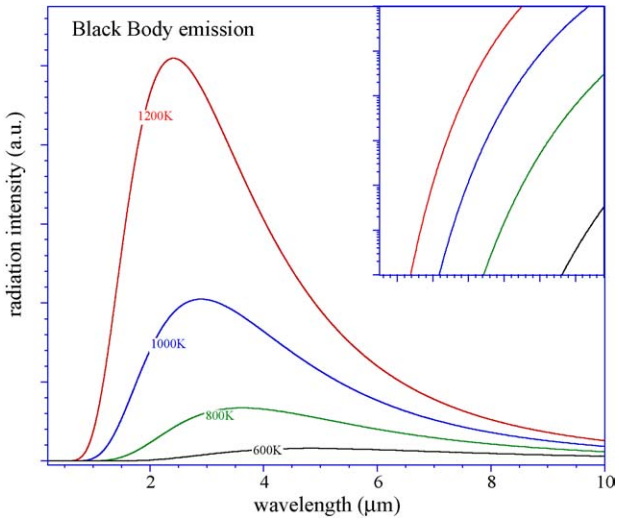

Fig. 2. Intensities and spectral distribution of a black body emitter such as a hot substrate for different temperatures. In inset depict on a logarithmic scale the onset the radiation for 100 and 600 K.

growth of In-rich group III-nitride alloys need to be explored in order to improve the structural and optical properties of InN and related alloys.

Recent studies in the indium-nitrogen system [10] show much uncertainty in the *p–T–x* relations due to missing experimental validation. However, studies of the nitrogen pressure required to prevent thermal decomposition of bulk InN, provide a relationship given by

$$p_{N_2} \rightarrow p_0 \exp\left[-\frac{\Delta H_r}{R}\left(\frac{1}{T}-\frac{1}{T_0}\right)\right], \quad (1)$$

which results in the p–T^{-1} relation shown in Fig. 1 [11]. This relation indicates that for the pressure range $p_{N_2} \leq 10^2$ bar and substrate temperatures ≤ 900 K, the surface decomposition of InN can be effectively suppressed.

The approach presented here explores the growth of indium-rich group III-nitrides at elevated pressures using InN as a model system in order to demonstrate the capabilities of high-pressure CVD. InN is the most challenging material system, since the equilibrium vapor pressure of nitrogen over InN is much higher compared to AlN and GaN [12]. A high-pressure flow channel reactor incorporating real-time optical characterization capabilities [13–16] is utilized to study and optimize InN nucleation and growth. At above atmospheric pressures, optical diagnostic techniques are uniquely suited to provide real-time information pertaining to gas flow dynamics in laminar and turbulent flow regimes. Optical diagnostics are also utilized to obtain crucial information regarding precursor flow and decomposition kinetics. Several optical techniques have been explored, but only a few provide the required robustness and sensitivity. For example, the substrate temperature during InN growth under high pressure is between 800 and 1000 K, resulting in a significant radiation emission, as shown in Fig. 2. Even if modulation techniques are applied, the intensity of the emitted radiation from to the substrate heater limits the sensitivity of many optical probe techniques operating in visible and infra-red (IR) ranges. As depicted in the inset of Fig. 2, the radiated intensity for a 1000 K back body emitter vanishes very quickly below 350 nm, with negligible contributions below 300 nm.

Utilizing ultraviolet absorption spectroscopic (UVAS) techniques as well as UV induced fluorescence spectroscopy to identify the group V and organometallic group III precursors in the gas phase is well established in the literature [17–20].

In the following sections, a brief introduction of the HPCVD reactor design is provided along with its real-time optical capabilities in order to characterize flow, gas phase and surface reactions. This is followed by three sections providing results on the optical characterization of the precursors trimethylindium (TMI) and ammonia (NH_3) and the optical monitoring of InN nucleation and overgrowth utilizing sequential precursor injection.

2. High-pressure reactor system

The growth of group III-nitrides at elevated pressures requires a completely redesigned OMCVD reactor system with special consideration directed towards flow kinetics, gas phase reactions, boundary layer diffusion and alteration of surface chemistry. This HPCVD reactor system utilizes a pulsed precursor injection technique, which is essential in order to achieve compression of the precursors to reactor pressure, minimization of gas phase reactions, optimization of nucleation kinetics, and analysis of gas phase and surface decomposition dynamics in real-time.

A symmetric arrangement of substrates in the upper and lower part of the flow channel is used, in order to prevent preferential material deposition on the opposite side of the heated substrate. As schematically depicted in Fig. 3b, optical access ports are integrated along the center axis of the substrates, which allows optical characterization of flow kinetics, gas phase reactions and the substrate surface through the back side. A more detailed description of the reactor design and the optical characterization capabilities is given elsewhere [13,16].

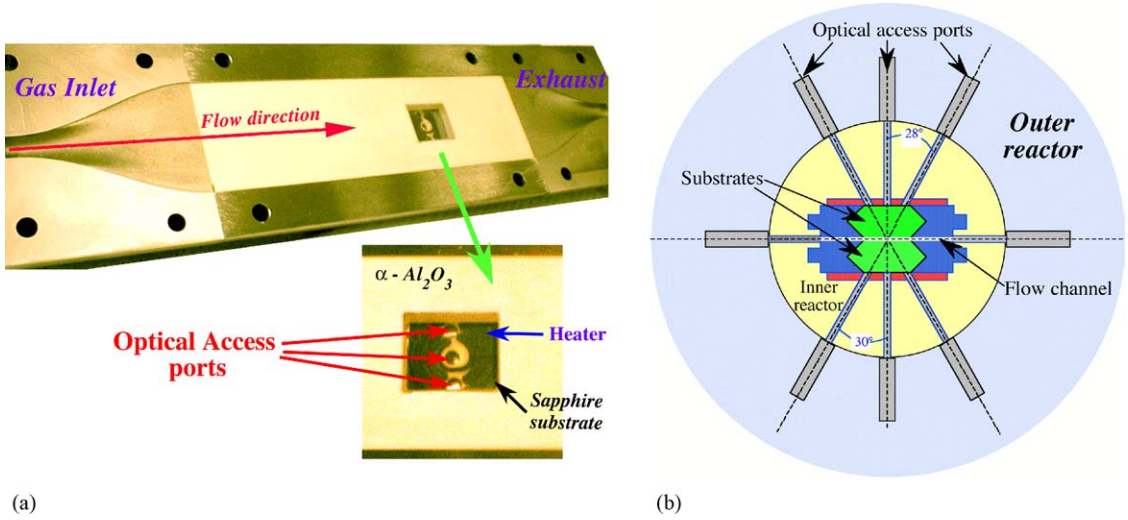

Fig. 3. (a) Half of the reactor flow channel assembly showing flow direction. The flow channel is designed with a constant cross-sectional area for the maintenance of laminar flow. The sapphire substrate is seen along center axis of flow and is held in two α-Al_2O_3 plates. (b) Schematic cross-section of the reactor containing the optical access ports and the center of the substrates. Two optical ports provide access to the flow channel and three ports in each of the two half sections of the reactor provide access to the growth surface.

The flow characteristics of the HPCVD reactor has been analyzed using laser light scattering, LLS, in a forward scattering geometry [21]. The onset of increased LLS scattering for pure nitrogen gas flow is summarized in Fig. 4a, indicating the flow and pressure ranges at which laminar flow can be maintained.

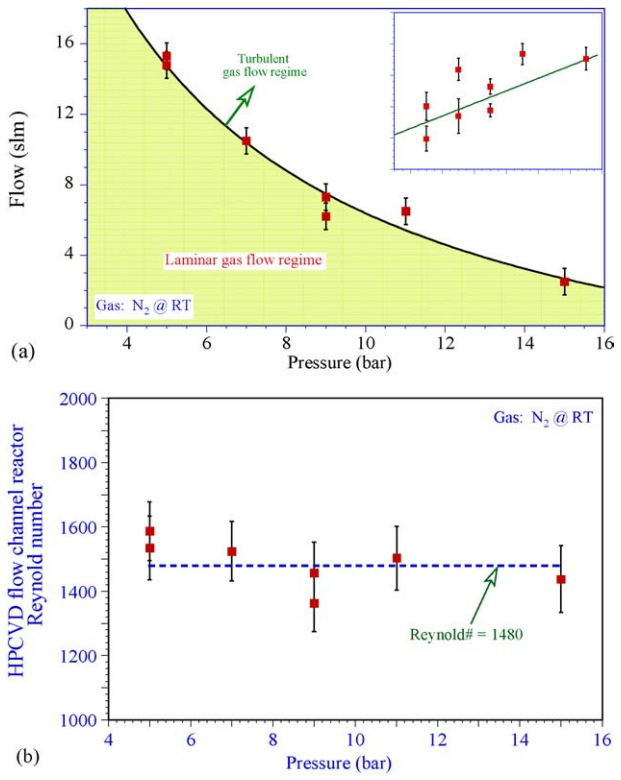

Fig. 4. (a) Transition from laminar to turbulent flow conditions as determined by LLS intensity measurements. The inset depicts the increase of the LLS with increasing pressure. (b) Calculated Reynolds numbers for HPCVD flow channel reactor with a cross-section of $A = 50\,\mathrm{mm}^2$.

The associated Reynolds number can be calculated via

$$Re = \frac{\rho u l}{\eta}, \tag{2}$$

where $\rho = 1.12\ (\mathrm{kg\,m^{-3}})$ is the density of the gas, 'u' the flow velocity, 'l' a flow reactor characteristic length parameter and $\eta = 1.8 \times 10^{-5}\ (\mathrm{kg\,m^{-1}\,s^{-1}})$ the dynamic viscosity. For ideal gases, a direct proportionality between the density of the gas and the pressure exists, which for a constant 'l' and η leads to a inverse proportionality between flow velocity and pressure. The calculated Reynolds numbers are shown in Fig. 4b with an average around 1480. No significant pressure dependency is observed.

3. Optical characterization of precursors and reactor flow characteristics

Transport of the TMI precursor from the bubbler to the gas flow control panel is achieved via a nitrogen carrier gas maintained at a temperature of 20 °C and pressure of 760 Torr. The actual molar flow rate of TMI is calculated from standard partial pressure curves (provided by the manufacturer) and nitrogen carrier gas flow rates and can be expressed as

$$n_{\mathrm{TMI}} = 8.3216 \times 10^{-9} \times x\,(\mathrm{mol\,s^{-1}}) \tag{3}$$

where x is the % full scale (%FS) setting of the carrier gas mass flow controller (100% FS = 500 sccm).

Initially, optical characterization of the TMI flux through the reactor flow channel is achieved under continuous flow conditions at near-atmospheric pressure, which does not require a compression stage. This carrier gas containing diluted TMI is combined with the main reactor nitrogen flow in the gas flow control panel and is directed to the reactor flow channel. The molar TMI:N_2 flow ratio χ through the reactor can be expresses

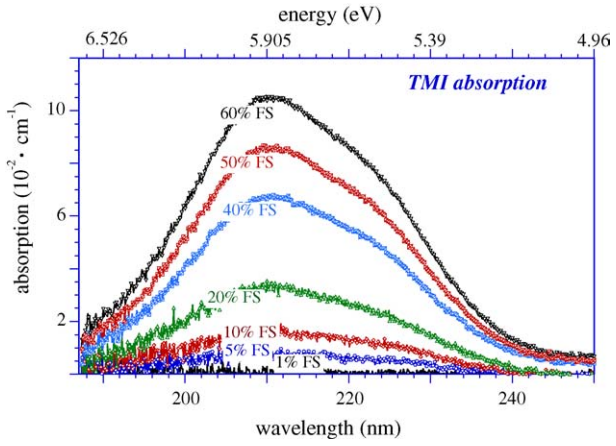

Fig. 5. Spectrally resolved absorption on TMI diluted in N_2 carrier gas as function of N_2-flow through TMI bubbler in %FS. The total flow through the reactor is maintained at 5 slm at 1630 mbar.

as

$$\chi = \frac{n_{\mathrm{TMI}}}{n_{\mathrm{total}}} = \frac{n_{\mathrm{TMI}}}{n_{\mathrm{Main\_N_2}} + n_{\mathrm{bubbler\_N_2}} + n_{\mathrm{TMI}}}$$

$$= \frac{2.237 \times 10^{-5} \times x}{z + 10^{-2} \times x + 2.237 \times 10^{-5} \times x} \quad (4)$$

where x and z are the percent full scale flow settings of the TMI carrier gas and main reactor N_2 mass flow controller settings, respectively.

The absorption of ultraviolet light as a function of TMI concentration has been characterized between 190 and 500 nm. A broad absorption feature in the wavelength range of 190–250 nm is observed at room temperature (RT) with the absorption peak centered at 210.7 nm. Fig. 5 shows the spectrally resolved absorption structure as a function of TMI carrier gas flow settings. For higher carrier gas flow settings, two absorption features centered at 210.7 and 221 nm can be observed. The center location of the strongest absorption feature remains constant at 210.7 nm for all TMI concentrations investigated. The maximum absorption and full-width-half maximum (FWHM) of this feature are shown in Fig. 6 as function of the TMI carrier gas mass flow controller setting while maintaining a reactor pressure of 1.6 bar and a total flow of 5 slm through the reactor. Analysis of this absorption feature provides a correlation between measured the absorption maxima and the TMI carrier gas flow setting, which can be expressed as $\alpha_{(x=\%\mathrm{FS})} = 1.72 \times 10^3$ (cm^{-1}).

Further analysis of the influence of the molar TMI flow ratio χ on this peak absorption maximum centered at 210.7 nm reveals an exponential relationship in the form of

$$\alpha_{(\chi)} = -0.37367 + 0.37282 \times \mathrm{e}^{\frac{\chi}{5.44\times10^{-4}}} \ (\mathrm{cm}^{-1}) \quad (5)$$

which is depicted in Fig. 7.

The combination of Eqs. (4) and (5) allow for real-time calculation of the flux of TMI molecules per unit time based on the observed ultraviolet absorption based upon

$$N_{\mathrm{TMI}} = \frac{10^{18}\, y\, (\ln(\alpha') - 2.28 \times 10^{-3})}{8.21 - 2\ln(\alpha')} \quad (6)$$

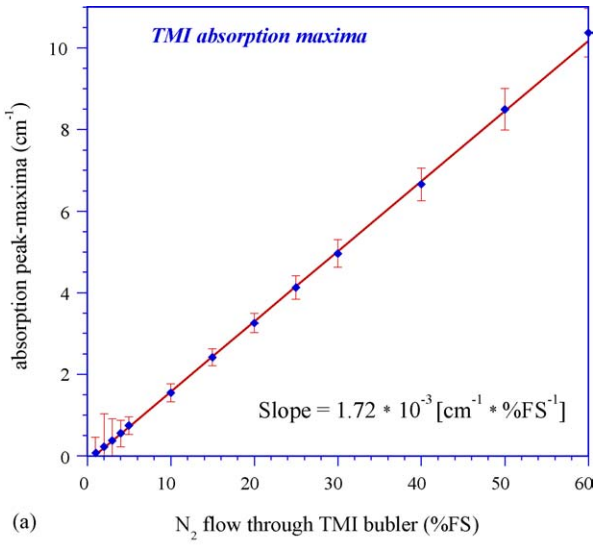

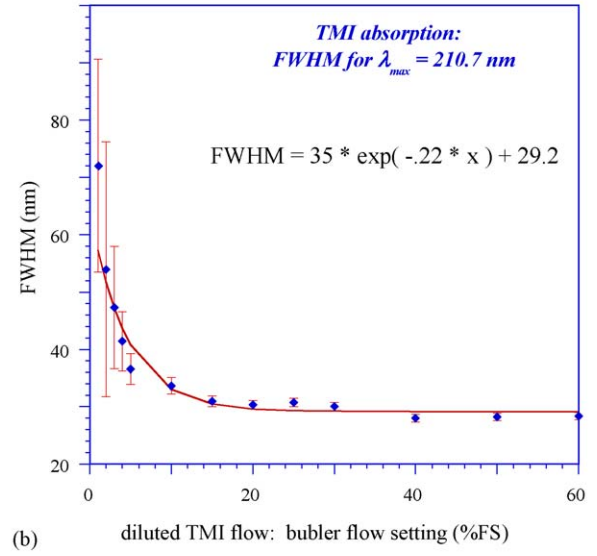

Fig. 6. (a) Absorption strength at $\lambda = 210.7$ nm as function of N_2 carrier gas flow through TMI bubbler in %FS. (b) FWHM for the absorption maximum at 213.5 nm.

where $\alpha' = \frac{\alpha + 0.37367}{0.37282}$ (cm^{-1}) and y is the %FS setting of the main nitrogen reactor flow. This result is used in the following section to compute the number of TMI molecules contained in a single pulse during TMI injection.

3.1. Optical characterization of pulsed TMI injection, diluted in N_2 carrier gas

In order to grow InN at above atmospheric pressures, a two-step process is employed for the injection of the precursors in to the HPCVD reactor flow channel. Initially, a 75 cm^3 reservoir at atmospheric pressure is filled with TMI diluted in N_2 carrier gas. In the second step, the reservoir is compressed by high-pressure nitrogen and injected into the main nitrogen flow. The filling of the reservoir, subsequent compression and injection in to the reactor, denoted as 'cycle sequence', is continually repeated.

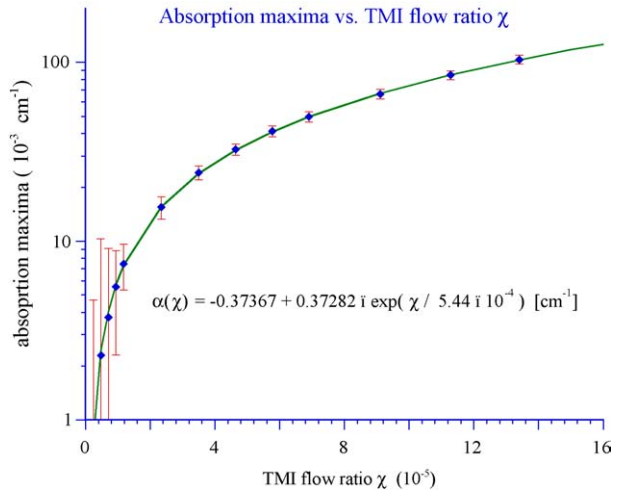

Fig. 7. Correlation of TMI absorption maximum and molar TMI flow ratio χ under steady-state flow conditions.

The cycle repetition rate, duration of the injection, as well as the temporal position of injection within a given cycle sequence are process parameters that are used to control gas phase reactions and the film growth process itself.

Fig. 8 shows real-time traces of the transmitted intensity monitored at 210.7 nm during pulsed TMI injection with a 6 s repetition rate for various TMI carrier gas flow rates. The reactor pressure is maintained at 1.6 bar with a total flow of all gases (TMI carrier gas and nitrogen main flow) through the reactor maintained at 5 slm. From the transmitted intensity traces, the associated absorption is computed, which can then be correlated to the molar TMI concentration contained in the each injected pulse.

Fig. 9 shows a typical trace for the absorption at 210.7 nm and the computed number of TMI molecules contained in the pulse. Analysis indicates that the sensitivity limit for TMI concentrations is on the order of 10 [14] TMI molecules per time unit depending on the reactor pressure and total flow rate.

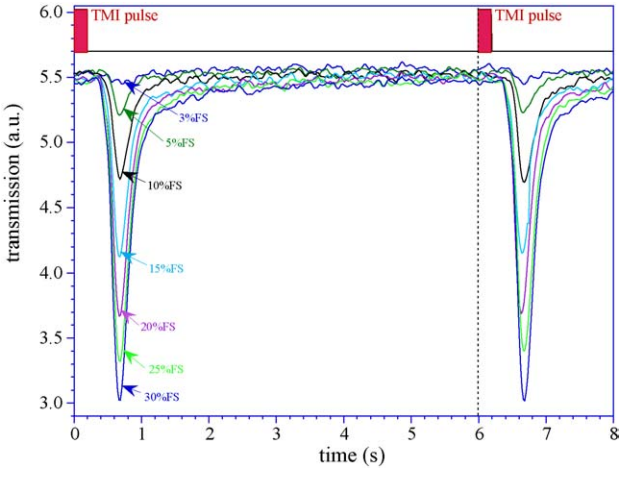

Fig. 8. Transmitted intensity trace monitored at 210.7 nm during TMI precursor pulse injection in the reactor at 1.6 bar and a total flow through the reactor of 5 slm. The TMI flow was varied from 15–150 sccm (3–30% FS). The cycle sequence is 6 s with a 0.2 s TMI pulse width.

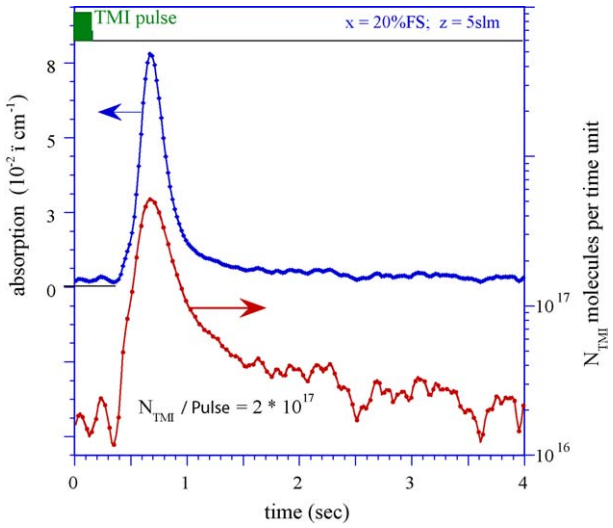

Fig. 9. UV absorption due to and concentration of TMI atoms (n_{TMI}) per unit time during pulsed TMI injection.

4. Optical characterization of ammonia (NH_3) precursor

Detailed characterization of the NH_3 flow dynamics and gas phase kinetics of NH_3 under HPCVD conditions has been previous published [30]. However, a brief summary of the characterization capabilities and analysis of the kinetics of NH is presented here. Similar to Section 3, the optical characterization of NH_3 is treated separately for continuous NH_3 flow and pulsed NH_3 injection. Under both continuous and pulsed flow conditions, the NH_3 vapor is transported from a NH_3 gas cylinder, which is regulated to deliver gas at 30 psi. An in-line filter is utilized in order to lower the concentrations of trace contaminants such as oxygen and water. Similar to the TMI flow analysis, the molar flow rate of NH_3 can be expressed as

$$n_{NH_3} = 7.4405 \times 10^{-6} \times y\,(\mathrm{mol\,s^{-1}}). \quad (7)$$

where y is the %FS scale setting of the NH_3 mass flow controller (100% FS = 1 slm). Under continuous flow conditions, the molar ammonia flow ratio χ through the reactor can be expressed as

$$\chi = \frac{n_{NH_3}}{n_{total}} = \frac{n_{NH_3}}{n_{Main\_N_2} + n_{NH_3}} = \frac{y}{50z + y} \quad (8)$$

where y and z are the % full scale settings of the NH_3 and main nitrogen mass flow controllers, respectively (100% FS(z) = 50 slm).

The flow of ammonia through the reactor has been characterized by UVAS in the wavelength range of 180–300 nm. Significant, concentration dependent absorption features are observed in the wavelength range of 190–240 nm. These absorption features are shown in Fig. 10 for various NH_3 mass flow controller settings with a 5 slm nitrogen main reactor flow of and a reactor pressure of 1.6 bar. The characteristic absorption features match previously reported data in literature [22,23]. The molar ammonia flow ratio χ required for the growth of InN is sufficiently high that several of the absorption lines are "saturated" at their peak value.

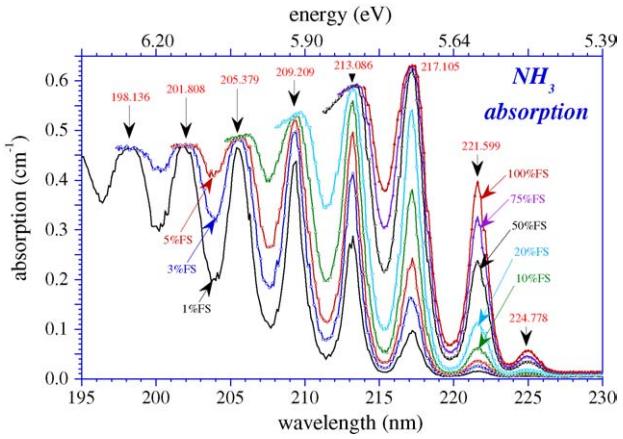

Fig. 10. Absorption spectra for various ammonia flows in %FS of the NH_3 mass flow controller diluted in 5 slm nitrogen main flow and a rector pressure of 1.6 bar.

For ammonia flow ratios in the range of $\chi = 1.0 \times 10^{-2}$ to 1.6×10^{-1}, the absorption feature centered at 221.6 nm is used in order to correlate the observed absorption and the NH_3 flow ratio χ through the reactor flow channel, as shown in Fig. 11. Analysis of this absorption feature, reveals the following relationship:

$$\alpha_{\text{peak\_217.1 nm}}(\chi) = 0.38\ \ln(\chi + 0.011) - 2.0\chi + 1.73\,(\text{cm}^{-1})$$
$$\alpha_{\text{peak\_221.6 nm}}(\chi) = -45 + 45.01\ \exp\left(\frac{\chi}{18}\right) \times 10^{-2}(\text{cm}^{-1}) \quad (9)$$

between the UV absorption and ammonia ratio χ.

The number concentration of NH_3 molecules per unit time can be computed as a function of the observed absorption. Considering the absorption feature at 221.6 nm, we find the NH_3 number concentration can be expressed as a function of the absorption α by

$$N_{\text{NH}_3(\lambda=221.6\,\text{nm})} = \frac{7.17 \times 10^{21} \times z\ \ln(\alpha')}{1 - 32\ \ln(\alpha')}\,(\text{s}^{-1})$$
$$\text{with}\ \alpha' = \frac{\alpha_{221.6\,\text{nm}} - 80}{80.01}. \quad (10)$$

The number concentration of NH_3 determined from Eq. (10) ($\lambda = 221.6$ nm) is plotted in Fig. 17b for NH_3 mass flow controller settings between 1 and 50% FS while maintaining a main reactor flow rate of 5 slm and a reactor pressure of 1.6 bar. Under continuous flow conditions, the ammonia concentration can be varied between 10 [19] and 2×10 [20] NH_3 molecules/s.

4.1. Optical characterization of pulsed ammonia injection

The flow of ammonia at higher pressures requires a compression and dilution stage in order to enable the injection of ammonia into the HPCVD reactor flow channel. As in the injection of the TMI precursor, a 75 cm^3 reservoir is filled at slightly above atmospheric pressure with ammonia gas, controlled by a mass flow controller (MFC) and a computer controlled filling time. In the following step, the reservoir is compressed with high-pressure N_2 up to the reactor pressure and injected into the reactor. Cycle repetition rate, duration of injection, and the position of injection can the adjusted with an accuracy of 1 ms.

Depending on the ammonia concentration per pulse injected into the reactor, several absorption features can be utilized to characterize and analyze the ammonia pulses. Fig. 12 shows typical absorption traces monitored at 221.6 nm during pulsed ammonia injection with a 6 s total cycle sequence time for various ammonia mass flow controller settings. The reactor pressure was maintained at 1.6 bar with a total gas flow through reactor at 5 slm.

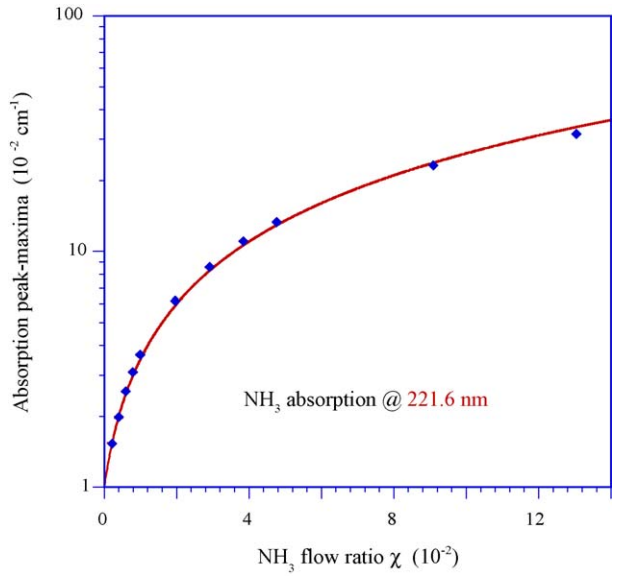

Fig. 11. Ammonia absorption monitored at $\lambda = 221.6$ nm as function of ammonia flow ratio χ under steady state flow conditions for a reactor pressure of 1.6 bar.

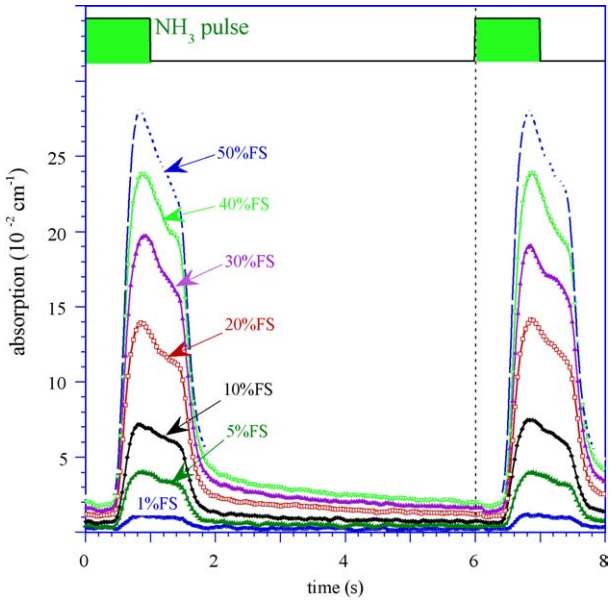

Fig. 12. Ammonia absorption traces monitored at $\lambda = 221.6$ nm for 1.0 s NH_3 pulses injected 6 s apart.

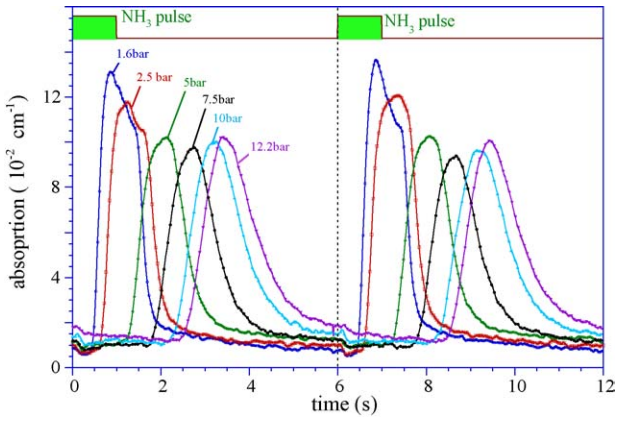

Fig. 13. Absorption traces monitored at λ = 221.6 nm for 1 s NH_3 pulses injected 6 s apart. The reactor main flow and the ammonia flow were kept constant at 5 slm nitrogen and 200 sccm, respectively.

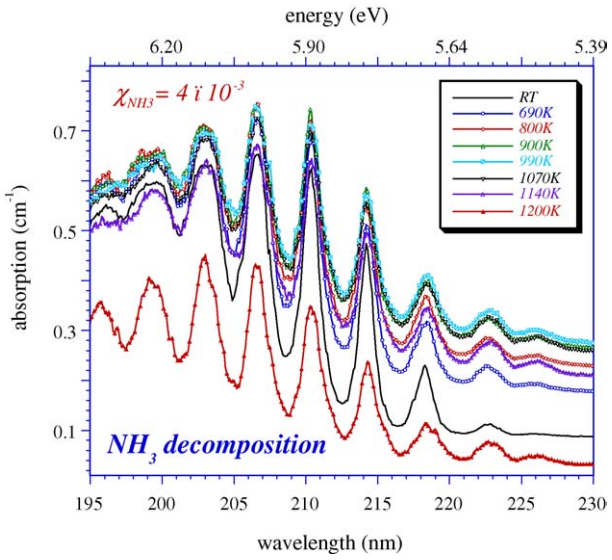

Fig. 14. Ammonia absorption spectra taken at different temperatures during steady state flow conditions for a reactor pressure of 1.6 bar.

The relationship between the absorption strength and ammonia number concentration provided by Eq. (10), together with the reservoir compression ratio and volume, the total number of ammonia molecules per pulse can be calculated.

The pulsed ammonia injection has been analyzed as function of pulse width, ammonia concentration per pulse, total reactor flow and reactor pressure. Fig. 13 shows the monitored absorption traces at λ = 221.6 nm for various reactor pressures, while maintaining a total gas flow through the reactor at 5 slm and ammonia flow of 200 sccm. It is important to note that for pressures above 10 bar, a carryover of ammonia from one cycle to the next is observed, resulting in an increase in the base line absorption of the overall absorption observed in the reactor flow channel.

Similar to the characterization of pulsed TMI injection, the pulsed ammonia injection monitored at the substrate centerline shows three distinct features. These pressure dependent features are (1) a systematic shift in the pulse arrival time, (2) a systematic ammonia pulse broadening and (3) a change in the NH_3 absorption cross-section for pressures larger 8 bar. These features have been analyzed in detail and are published elsewhere [30].

5. Decomposition dynamics of TMI and ammonia precursors

The decomposition dynamics of ammonia has been analyzed in the temperature range of 300–1200 K under continuous ammonia flow conditions at a reactor pressure of 1.6 bar. Fig. 14 shows the temperature dependence of ammonia spectra recorded between 180 and 230 nm for a molar ammonia flow ratio $\chi = 4 \times 10^{-3}$. The increase of the nitrogen absorption base line as function of the temperature has been accounted for. The spectroscopic scan between 180 and 400 nm revealed no new absorption feature that could be associated with ammonia fragments at higher temperatures.

Above 990 K, a significant reduction in the absorption strength is observed, indicating the onset of the decomposition of ammonia in the reactor flow channel. The change in the absorption peak maxima as a function of temperature as is shown in Fig. 15a for a molar ammonia flow ratio χ of 10^{-2}.

The absorption peak maxima increase as the temperature raises due to the change in the absorption cross-section. Above 900 K, a plateau is observed with a strong fall-off above 1100 K. The decomposition dynamics at higher reactor pressures were studied during pulsed ammonia injection as a function of temperature, as depicted in Fig. 15b. Starting around 850 K, a fall-off in the peak absorption amplitude can be observed, which is at a slightly lower temperature as observed at 1 bar reactor pressure and the same total flow. Since the gas flow velocity in the reactor system decreases inversely with pressure, an additional temperature effect due to the reduced gas velocity at higher pressures must be considered.

The decomposition dynamics for TMI were studied only for pulsed TMI injection at higher reactor pressures, in order to avoid the formation of atomic indium on the windows at higher temperatures. Fig. 16 shows the observed changes in the amplitude of peak maximum absorption at 210.7 nm. The onset of TMI decomposition in the gas phase occurs around 800 K, which is slightly higher than those reported under low-pressure OMCVD conditions [18,24] for the growth of group In–V compounds [25,26].

6. Real-time optical characterization of InN growth: nucleation and overgrowth

An understanding of the decomposition kinetics of precursors utilized in OMCVD growth techniques is crucial to precise engineering of both nucleation and subsequent film growth. Detailed modeling of the expected precursor flow dynamics and chemical kinetics under HPCVD conditions has been previously published [15]. The decomposition studies for ammonia in the previous section suggest temperatures above 1000 K are required for sufficient cracking of the ammonia precursor for the growth of InN. However, literature data for InN growth

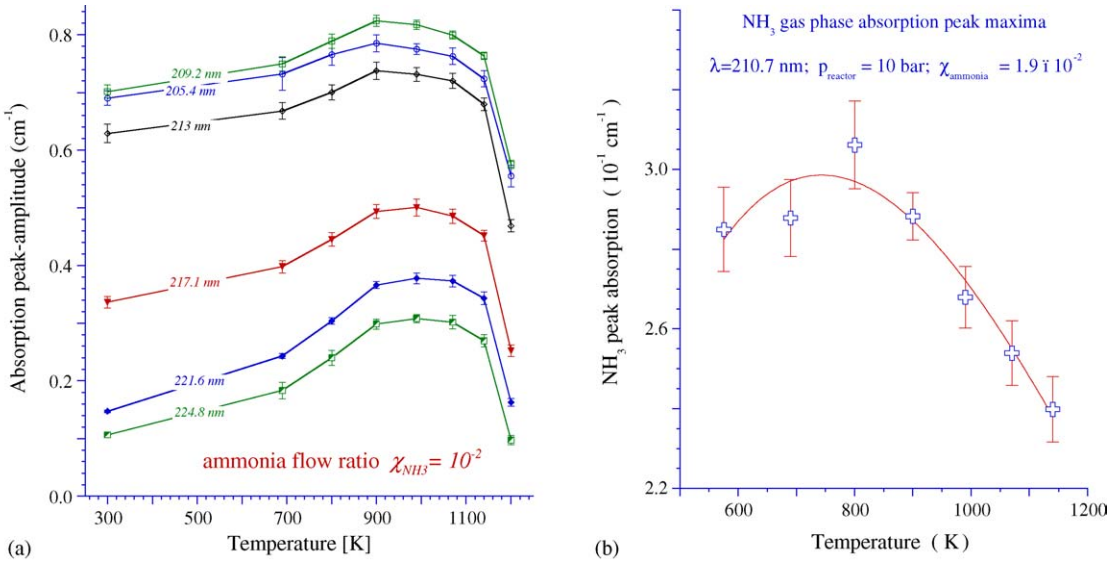

Fig. 15. (a) Change of the ammonia absorption peak maxima as function of temperature. (b) Decomposition of ammonia during pulsed precursor injection at a reactor pressure of 10 bar.

by OMCVD indicate a growth temperature of 675–750 K [24], 775 K [25] and 810–840 K [26]. Under HPCVD conditions, we can expect to be able to increase the growth temperature about 50–100 K higher than possible at low-pressure OMCVD conditions. However, this still leaves a temperature mismatch between optimum ammonia decomposition and optimal InN growth temperature, which remains a challenge to be solved. For low-pressure OMCVD growth techniques, TMI:NH_3 ratios of 1:10 [4] and larger [24,25] are required to counteract the low ammonia decomposition rate at optimum growth temperatures.

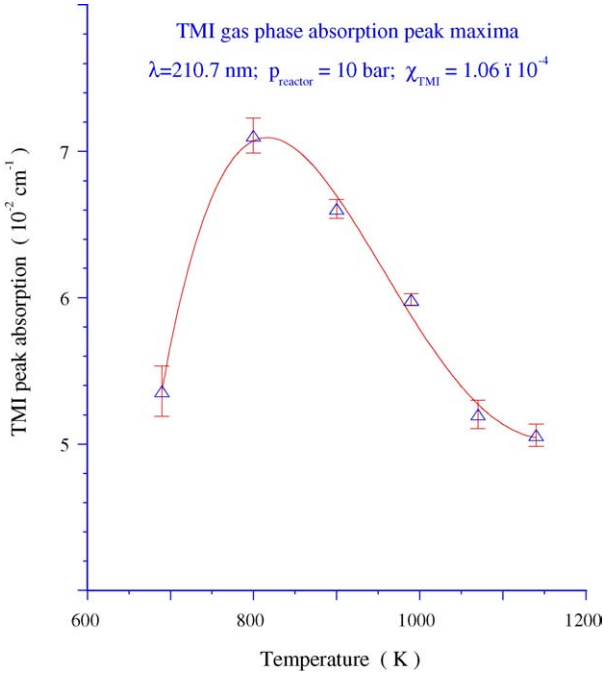

Fig. 16. Decomposition of TMI at 10 bar reactor pressure, monitored during pulsed TMI injection as function of temperature.

Here, the growth of InN is achieved by exposing the substrate surface to pulses of TMI [$In(CH_3)_3$] and ammonia [NH_3] at 800–1050 K. The symmetrically embedded sapphire crystals with a (0 0 0 1) growth surface are heated to 1150 K and exposed to ammonia for typically 30 min. After the nitrification of the sapphire surface, the temperature is lowered to the growth temperature, and the InN growth is initiated.

The growth of InN is initiated by supplying pulses of the precursors that are sequentially separated by pauses as shown schematically in Fig. 17. As discussed in the previous sections, the TMI and NH_3 pulses are temporally controlled and embedded in a nitrogen gas main flow through the reactor. The total flow through the reactor as well as the reactor pressure are kept constant.

This growth at elevated-pressures has an extended growth parameter space as compared to low-pressure organometallic chemical vapor deposition. Growth parameters that need to be evaluated are reactor pressure, average gas velocity, TMI and ammonia pulse separation and reaction time, the molar TMI to ammonia, $R_{TMI:NH_3}$ and growth temperature.

This large parameter space requires the application of real-time optical monitoring techniques in order to access the nucleation and growth conditions and in order to optimize the growth

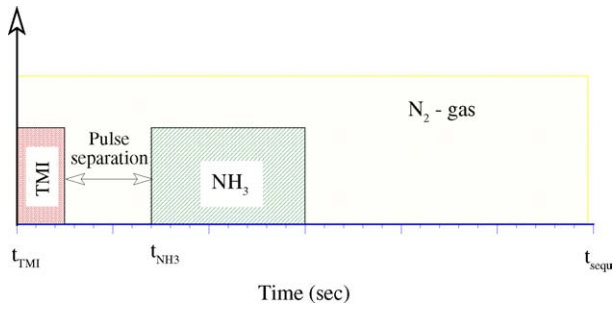

Fig. 17. Schematic representation of a precursor cycle sequence used for the growth of InN via the precursors TMI and ammonia.

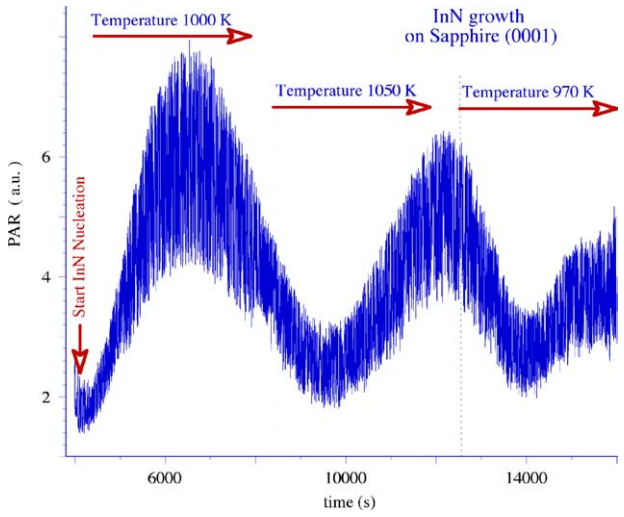

Fig. 18. Monitoring of InN growth by PAR for 2.5 interference fringes.

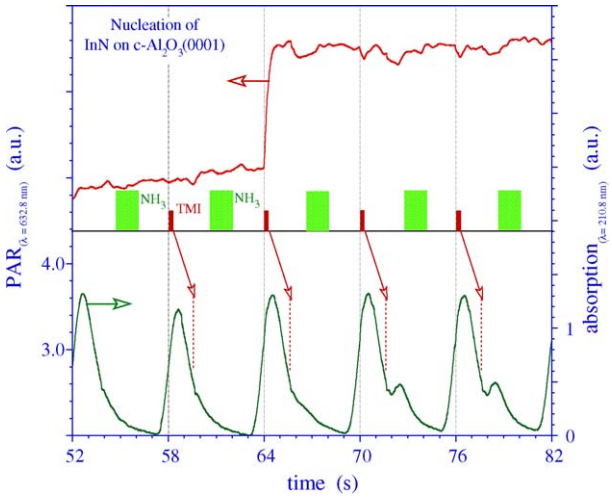

Fig. 19. Monitoring of InN nucleation by PAR and UV absorption. A precursor cycle sequence of 6 s with 0.4 s TMI and 1.4 s ammonia pulses, separated by 1.4 s were used.

parameters. For monitoring InN nucleation and growth, single wavelength principal angle reflectance (PAR) [13,30] and laser light scattering is applied, employing a p-polarized light beam ($\lambda = 6328$Å) and a Glan-Thompson prism. The beams impinge on the substrates at an angle of incidence $\varphi = 30^\circ$ and 28° for the upper and lower part, respectively. The reflected beams are detected by Si photodiodes. The intensity of the scattered radiation is monitored simultaneously by a photo multiplier tube (PMT) located perpendicular to the plane of incidence. PAR is based on the same principle as p-polarized reflectance spectroscopy [27–29]. However, PAR utilizes p-polarized light impinging the substrate–ambient interface near the principal angle φ_P. corresponding to the pseudo-Brewster angle φ_B for p-polarized light impinging the ambient–substrate interface. Depending on the substrate temperature and laser wavelength, the principal angle φ_P. varies from 27.5° to 30° for the sapphire–ambient interface [13]. The angle of total reflection, φ_T, is approximately 5° above φ_P.

Fig. 18 shows the PAR trace recorded for the wavelength $\lambda = 6328$ Å, during InN growth. Superimposed on the interference oscillations of the reflected intensity is a fine structure that is strongly correlated to the time sequence of the supply of precursors employed. Each peak in the fine structure corresponds to a complete precursor cycle sequence.

Fig. 19 shows typical observed PARS and UVAS monitored during nucleation on InN. The lower trace shows the UVAS trace recorded for the wavelength $\lambda = 210.8$ nm, monitoring the un-decomposed ammonia and TMI species above the growth surface. The PAR trace in the upper half of the figure is recorded for the wavelength $\lambda = 6328$ Å, monitoring with high sensitivity the changes in the dielectric function of the substrate–ambient interface. Also indicated are the positions of the pulsed precursor injection with a total cycle sequence time of 6 s. Note that the precursor injection time and the response seen in UVAS and PAR are temporal shifted according to the average gas velocity in the reactor which is a result of the time lag between the opening of the injection valve and the arrival of the precursors at the centerline of the substrate in the reactor flow channel.

Prior to growth, the surface is exposed only to pulses of ammonia. The growth of InN is initiated with the first TMI pulse at 58 s followed by an ammonia pulse 1.4 s later. Fig. 20 clearly shows the time delay of the pulses from the injection point until they reach the centerline of the substrate. About one to two cycle sequences elapse before the UV absorption trace of TMI is clearly observed (see arrows). The PAR signal shows a large jump after the ammonia pulse reaches the substrate, indicating the start of nucleation of InN and the present of TMI fragments in the surface vicinity. During the first few growth sequence cycles, the PAR signal shows growth related oscillations that are not well developed. The growth temperature is 990 K, a reactor pressure of 10 bar, a total flow of 5 slm, and a molar ratio TMI to ammonia, $R_{TMI:NH_3}$ of 1:500.

Steady state surface chemistry is reached after 5–20 cyclic precursor injections, depending on substrate temperature, precursor flow ratio, gas phase velocity and reactor pressure. As depicted in Fig. 20, a periodic modulated PAR signal is observed

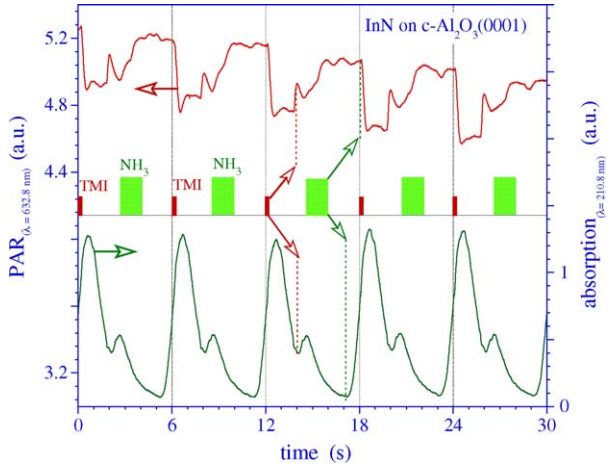

Fig. 20. PAR and UV absorption traces during steady-state InN growth at 990 K. The rector pressure was 10 bar with a total flow of 5 slm. The overall decrease in the PAR signal corresponds to InN growth.

under steady-state growth conditions where the signatures found in the PAR signal can be directly correlated to the present of ammonia an TMI fragments in a surface layer and at the growth surface. The overall decrease in the PAR signal intensity correlates to the InN growth per cycle sequence as discussed in detail for p-polarized reflectance [29]. The signatures observed in UV absorption trace coincide with the PAR response, even though the nature of these responses is different.

As the temperature is lowered from 940 to 840 K, the amplitude of the growth related PAR (not shown) signal becomes smaller and less pronounced. At 840 K, the growth related features indicate no growth due to inefficient decomposition of ammonia and TMI in the gas phase and surface reaction layer. This result agrees with the decomposition dynamics shown in Fig. 15 for ammonia.

Monitoring the PAR, LLS and UVAS responses during various growth conditions provides crucial information on the gas phase decomposition dynamics of the precursor and the subsequent diffusion through the surface boundary layer to the growth surface. The establishment of an optical data base as function of reactor pressure, flow velocity, molar III:V ratio and growth temperature will provide the base for a more detailed understanding on the dissociation of the precursors ammonia and TMI and of reaction rate constants for growth of InN as theoretical predicted by Cardelino et al. [15].

6.1. Ex situ InN layer characterization

The structural properties of epitaxially grown InN films have been investigated using X-ray diffraction. Fig. 21 shows typical XRD spectra recorded in the ω–2θ mode for samples #22L, #24L and #25L. These samples were grown at a temperature of 850 °C with a reactor pressure of 11 bar and average gas flow velocity of 45 cm/s. The precursors ratio, $R_{NH_3:TMI}$, for samples #22L, #24L and #25L was set at 8000, 1000 and 410, respectively, Sample #22L shows a broad reflection from wurtzite-type InN centered at 31.26° with a full-width at half maximum (FWHM) of 650 arcsec. This indicates a structural quality that is equivalent to InN thin films grown on GaN/AlN buffer layers, which have been produced by MBE growth methods [31]. As the precursor ratio $R_{NH_3:TMI}$ is lowered from 8000 to 1000 (sample #24L) the InN (0 0 2) reflection broadens and shifted lower to 31.2°. In addition, the InN (1 0 1) reflection centered at 31.1° becomes more pronounced. For $R_{NH_3:TMI}$ at 200 (sample #25L), both the InN (0 0 2) and InN(1 0 1) reflections show double structures, indicating the existence of additional InN related phases with FWHM less than 200 arcsec in very close proximity.

Analysis of the spectra for samples #22U and #25L reveal the lattice constants $a = 3.557$ Å and $c = 5.754$ Å. These values are in close proximity to previous reported lattice constants for high quality InN [32]. It is important to note, however, that the asymmetric line suggest the existence of additional phases in close proximity to the main InN reflections, the origin of which is presently under investigation.

Fig. 22 shows the optical absorption spectra in the energy range from 3 to 0.5 eV for a set of typical InN thin films grown under HPCVD conditions. For all samples shown, the layers

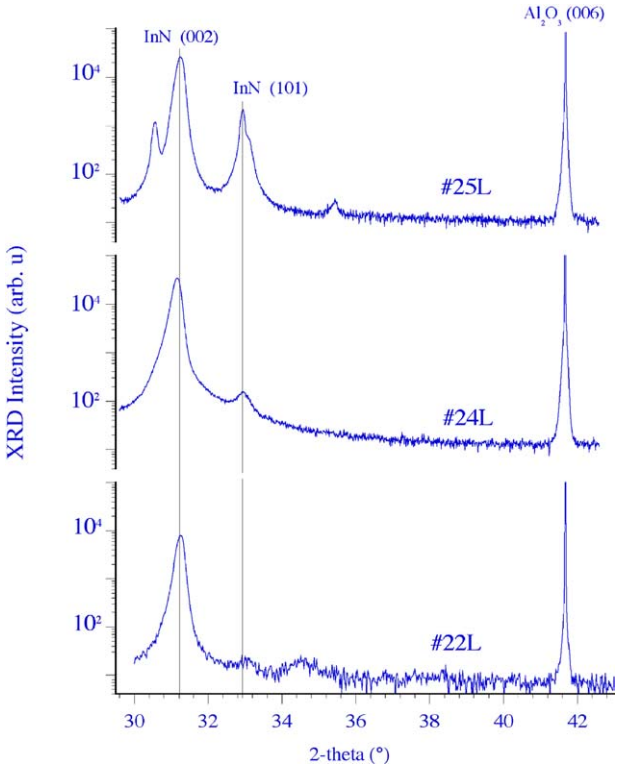

Fig. 21. Results of XRD measurements of InN on Sapphire (0 0 0 1). Precursor flow ratio, $R_{NH_3:TMI}$, employed during growth of samples #22L, #24L and #25L was 8000, 1000 and 200, respectively.

were grown at a reactor pressure of 15 bar, a gas flow velocity of 50 cm/s and temperature of 850 °C. The precursor flow ratio $R_{NH_3:TMI}$ was maintained at 3900, 2800, 1000 and 420 for samples #31L, #37U, #24L and #30L, respectively. Note that all samples, regardless of $R_{NH_3:TMI}$ exhibit an absorption feature centered at 0.63 eV. This feature has been attributed to plasmon excitations in the conduction band [33] due to a large free

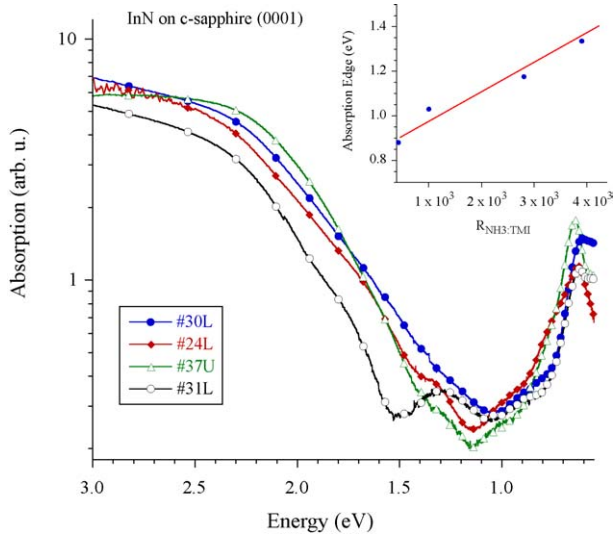

Fig. 22. Absorption spectra for characteristic InN samples grown with different ammonia to TMI ratio. The inset shows the absorption band edge as a function of ammonia to TMI precursor flow ratio.

carrier concentration. Since this feature remains unchanged in position and strength, our data suggest that the absorption edge shift towards lower energies is not directly related to the free carrier concentration, but rather to stoichiometry variations in InN.

The large variation in the absorption structures exhibited by these samples suggest that the observed absorption shift from approximately 1.3 to 0.83 eV are governed by a series of absorption structures centered at 0.87, 1.1 and 1.3 eV. Numerical analysis of these features has been used to examine the dominant absorption band edge beginning at 2.5 eV as a function of the $R_{NH_3:TMI}$, the results of which are shown in the inset of Fig. 22. The correlation between optical absorption edge shift and the precursor flow ratio $R_{NH_3:TMI}$ indicated a close correlation between the precursor flow ratio and film stoichiometry.

7. Conclusion

The growth of epitaxial InN layers by high-pressure chemical vapor deposition has been explored in the laminar flow regime, evaluating the growth parameter for reactor pressures in range of 10–15 bars, gas flow velocities from 20 to 50 cm s^{-1}, and molar ammonia to TMI ratios between 400 and 8000. The flow and decomposition kinetics of the precursors ammonia and TMI have been studied by ultraviolet absorption spectroscopy under pulsed precursor injection. UVAS, principal angle reflectance and laser light scattering have been applied to study the growth of epitaxial InN layers under high-pressure chemical vapor deposition conditions. As demonstrated, the combination of UVAS, PAR and LLS allow the characterization of gas phase chemistry as well as highly sensitive studies of surface processes during InN nucleation and steady-state InN growth, which will be essential for engineered nano-scale device structures. The link between the surface sensitive PARS response to the real-time gas phase analysis (UVAS) will enable the formulation of a comprehensive growth model, providing crucial insights in the gas phase decomposition kinetics, surface chemistry processes, and film growth processes at high pressures.

Epitaxial InN growth has been achieved in the flow range of 8–12 slm with $R_{TMI:NH_3}$ varying from 1:400 to 1:8000 at growth temperatures of approximately 850 °C. The ex situ InN layer characterization indicates that the shift of the absorption edge from 1.8 eV down to approximate 0.7 eV is closely related to the precursor flow ratio and with it to stoichiometry of the InN layer. The structural characterization of the InN thin films by XRD found reflection features indicating both the presence of high quality InN and a strong dependence of these features on the precursor flow ratio. The initial results suggest that the optimum molar flow ratio, ammonia to TMI, under HPCVD conditions might be below 400, which is due to the efficient cracking of the nitrogen precursor at the high reactor pressure and high growth temperature. Further studies varying the ammonia to TMI flow ratio, the center flow velocity, and the growth temperatures will be needed to access the optimum growth window. Due to the good match with the GaN/AlN processing windows, HPCVD will be a valuable tool to explore indium-rich group III-nitride alloys and heterostructures.

Acknowledgments

We would like to acknowledge support of this work by NASA grant NAG8-1686, DOD MURI Grant F-49620-95-1-0447, the collaborative support by Prof. Ferguson's research group at Georgia Institute of Technology, and support through GSU-RPE.

References

[1] A.G. Bhuiyan, A. Hashimoto, A. Yamamoto, J. Appl. Phys. 94 (5) (2003) 2779–2808.
[2] V.Yu. Davydov, A.A. Klochikhin, Semiconductors 38 (8) (2004) 861–898.
[3] Z. Sitar, M.J. Paisley, B. Yan, J. Ruan, W.J. Choyke, R.F. Davis, J. Vac. Sci. Technol. B8 (1990) 316.
[4] J.M. Van Hove, G. Carpenter, E. Nelson, A. Wowchak, P.P. Chow, J. Cryst. Growth 164 (1996) 154–158.
[5] V.Yu. Davydov, A.A. Klochikhin, V.V. Emtsev, D.A. Kurdyukov, S.V. Ivanov, V.A. Vekshin, F. Bechstedt, J. Furthmüller, J. Aderhold, J. Graul, A.V. Mudryi, H. Harima, A. Hashimoto, A. Yamamoto, E.E. Haller, Phys. Status Solidi B 234 (3) (2002) 787–795.
[6] F.-H. Yang, J.-S. Hwang, K.-H. Chen, Y.-J. Yang, T.-H. Lee, L.-G. Hwa, L.-C. Chen, Thin Solid Films 405 (1–2) (2002) 194–197.
[7] V.Ya. Malakhov, Sol. Energy Mater. Sol. Cells 76 (4) (2003) 637–646.
[8] E. Kurimoto, M. Hangyo, H. Harima, M. Yoshimoto, T. Yamaguchi, T. Araki, Y. Nanishi, K. Kisoda, Appl. Phys. Lett. 84 (2) (2004) 212–214.
[9] V.Yu. Davydov, A.A. Klochikhin, V.V. Emtsev, A.V. Sakharov, S.V. Ivanov, V.A. Vekshin, F. Bechstedt, J. Furthmüller, J. Aderhold, J. Graul, A.V. Mudryi, H. Harima, A. Hashimoto, A. Yamamoto, J. Wu, H. Feick, E.E. Haller, in: Zhores I. Alferov, Leo Esaki (Eds.), Proceedings of the 10th International Symposium on Nanostructures: Physics and Technology, vol. 5023, SPIE, 2003, pp. 68–71.
[10] B. Onderka, J. Unland, R. Schmid-Fetzer, J. Mater. Res. 17 (2002) 3065–3083.
[11] J.B. McChesney, P.M. Bridenbaugh, P.B. O'Connor, Mater. Res. Bull. 5 (1970) 783–791.
[12] O. Ambacher, M.S. Brandt, R. Dimitrov, T. Metzger, M. Stutzmann, R.A. Fischer, A. Miehr, A. Bergmajer, G. Dollinger, J. Vac. Sci. Technol. B 14 (6) (1996) 3532–3542.
[13] N. Dietz, S. McCall, K.J. Bachmann, Proceedings of the Microgravity Conference 2000, Huntsville, AL, June 6–8, NASA/CP-2001-210827, 2001, pp. 176–181.
[14] S.D. McCall, K.J. Bachmann, in: J.E. Northrup, J. Neugebauer, S.F. Chichibu, D.C. Look, H. Riechert (Eds.), Mater. Res. Soc. Symp. Proc., vol. 693, 2002, pp. I3.13.1–I3.13.8.
[15] B.H. Cardelino, C.E. Moore, C.A. Cardelino, S.D. McCall, D.O. Frazier, K.J. Bachmann, J. Phys. Chem. A 107 (19) (2003) 3708–3718.
[16] N. Dietz, V. Woods, S. McCall, K.J. Bachmann, Proceedings of the Microgravity Conference 2002, NASA/CP-2003-212339, 2003, pp. 169–181.
[17] G.A. Hebner, K.P. Killeen, R.M. Biefeld, J. Cryst. Growth 98 (3) (1989) 293–301.
[18] G.A. Hebner, K.P. Killeen, J. Appl. Phys. 67 (3) (1990) 1598–1600.
[19] H. Okabe, M.K. Emadi-Babaki, V.R. McCrary, J. Appl. Phys. 69 (3) (1991) 1730–1735.
[20] M.C. Johnson, K. Poochinda, N.L. Ricker, J.W. Rogers Jr., T.P. Pearsall, J. Cryst. Growth 212 (1–2) (2000) 11–20.
[21] V. Woods, H. Born, M. Strassburg, N. Dietz, J. Vac. Sci. Technol. A 22 (4) (2004) 1596–1599.
[22] J.A. Syage, R.B. Cohen, J. Steadman, J. Chem. Phys. 97 (9) (1992) 6072–6084.
[23] F.Z. Chen, D.L. Judge, C.Y. Robert Wu, J. Caldwell, Planet. Space Sci. 47 (1–2) (1998) 261–266.
[24] Z.X. Bi, R. Zhang, Z.L. Xie, X.Q. Xiu, Y.D. Ye, B. Liu, S.L. Gu, B. Shen, Y. Shi, Y.D. Zheng, Mater. Lett. 58 (27–28) (2004) 3641–3644.

[25] T. Schmidtling, M. Drago, U.W. Pohl, W. Richter, J. Cryst. Growth 248 (2003) 523–527.
[26] A. Jain, S. Raghavan, J.M. Redwing, J. Cryst. Growth 269 (1) (2004) 128–133.
[27] N. Dietz, K.J. Bachmann, Vacuum 47 (1996) 133–140.
[28] N. Dietz, V. Woods, K. Ito, I. Lauko, J. Vac. Sci. Technol. A 17 (4) (1999) 1300–1306.
[29] N. Dietz, Mater. Sci. Eng. B 87 (1) (2001) 1–22.
[30] N. Dietz, V. Woods, M. Strassburg, J. Vac. Sci. Technol. A 23 (4) (2005) 1221–1228.
[31] K.M. Yu, Z. Liliental-Weber, W. Walukiewicz, W. Shan, J.W. Ager III, S.X. Li, R.E. Jones, E.E. Haller, Hai Lu, J.S. William, Appl. Phys. Lett. 86 (2005) 071910.
[32] A. Wakahara, A. Yoshida, Appl. Phys. Lett. 54 (8) (1989) 709–711.
[33] D.B. Haddad, J.S. Thakur, V.M. Naik, G.W. Auner, R. Naik, L.E. Wenger, Mater. Res. Soc. Symp. Proc. 743 (2003) L11–L22.